Design and Analysis of a Three-Phase Wireless Charging System for Lightweight Autonomous Underwater Vehicles

Tianze Kan, *Student Member, IEEE*, Ruikun Mai, *Member, IEEE*, Patrick P. Mercier, *Member, IEEE*, and Chunting Chris Mi, *Fellow, IEEE*

***Abstract*—Lightweight autonomous underwater vehicles (AUVs), powered by rechargeable batteries, are widely deployed in inshore surveying, environmental monitoring, and mine countermeasures. While providing valuable information in locations humans have difficulty accessing, limited battery capacity of such systems prevents extended mission times. In order to extend mission times, this paper proposes a three-phase wireless charging system that could be used in a field-deployable charging station capable of rapid, efficient, and convenient AUV recharging. Wireless charging should not, however, affect instrumentation located inside the AUV. Thus, a three-dimensional finite element analysis tool is employed to study the characteristics of magnetic fields inside the AUV during three-phase charging. Simulation results reveal that the magnetic field generated by the proposed three-phase coil structure is concentrated away from the center of the AUV, where instrumentation would nominally be located. Detailed circuit analysis and compensation method to achieve resonance on both transmitter's and receiver's sides are also given. To validate the proposed concept, a three-phase wireless charging system is developed. Experimental results demonstrate that the system is able to transfer 1.0 kW with a dc–dc efficiency of 92.41% at 465 kHz.**

***Index Terms*—Autonomous underwater vehicles (AUVs), coil design, three-phase system, wireless power transfer.**

I. Introduction

THE concept of wireless power is originated from Hertz and well known by the work of Tesla [1], [2]. Today the applications of wireless power transfer can be found in charging biomedical implants, consumer electronics, electric vehicles, and autonomous underwater vehicles (AUVs) [3]–[17].

Lightweight AUVs are typically deployed in applications such as inshore surveying, environmental monitoring, and mine countermeasures, and provide highly valuable data and information in location where humans may not be able to access. Unfortunately, the limited capacity of on-board rechargeable batteries cannot sustain sufficiently long mission times. AUVs are, thus, required to go back to their base station, get charged, and return to its mission afterward. There are two conventional charging options: conductive charging and battery swapping. Conductive charging, in which a physical connection between the charging station and the AUV is established, is efficient and straightforward. However, it is necessary to provide a hermetic seal along the connection electrodes, which can be difficult when making connections in seawater. Battery swapping, in which a discharged battery is replaced by a fully charged one, effectively shortens the charging time and the AUV could be back to mission immediately. However, it requires complex battery insertion and retrieval mechanisms [13]. Moreover, frequent battery swapping results in problems on AUV's airtightness.

In order to provide a convenient and safe charging option for AUVs, Feezor *et al.* [14] proposed wirelessly charging an AUV at its underwater docking station via alternating magnetic fields with no physical connection. Periodic wireless charging was able to extend the AUV's mission tournament time. Since then, McGinnis *et al.* [15] developed a wireless charging system for AUVs to transfer 240 W power with 70% dc–dc efficiency. Li *et al.* [16] studied the effects of gap distances between the transmitter and the receiver and designed a 400 W system with approximately 90% efficiency at a gap distance of 2 mm. Unfortunately, in those designs, the receivers were directly mounted to the AUV's hull, which affected the shape of AUV's hull. As a result, the speed and the mission turnaround time of the AUV would be shortened accordingly. To address this, Shi *et al.* [17] introduced a coaxial coil structure, in which the receiver coil with a small thickness was mounted around the AUV's hull. It had fewer effects on the shape of the AUV's hull since the coil structure was well fitted with the AUV's hull. However, the drawback was that the generated magnetic field diverged and was very possible to affect the existing electronics devices in the AUV during charging. Therefore, one of the main challenges

Manuscript received May 6, 2017; revised August 25, 2017; accepted September 14, 2017. Date of publication September 26, 2017; date of current version April 20, 2018. This work was supported by the U.S. Department of Energy Graduate Automotive Technology Education Grant. Recommended for publication by Associate Editor J. A. Pomilio. *(Corresponding author: Chunting Chris Mi.)*

T. Kan is with the Department of Electrical and Computer Engineering, San Diego State University, San Diego, CA 92182 USA, and also with the Department of Electrical and Computer Engineering, University of California San Diego, La Jolla, CA 92093 USA (e-mail: tikan@eng.ucsd.edu).

R. Mai is with the Department of Electrical Engineering, Southwest Jiaotong University, Chengdu 610031, China (e-mail: 82009003@qq.com).

P. P. Mercier is with the Department of Electrical and Computer Engineering, University of California San Diego, La Jolla, CA 92093 USA (e-mail: pmercier@ucsd.edu).

C. C. Mi is with the Department of Electrical and Computer Engineering, San Diego State University, San Diego, CA 92182 USA (e-mail: mi@ieee.org).

Color versions of one or more of the figures in this paper are available online at http://ieeexplore.ieee.org.

Digital Object Identifier 10.1109/TPEL.2017.2757015

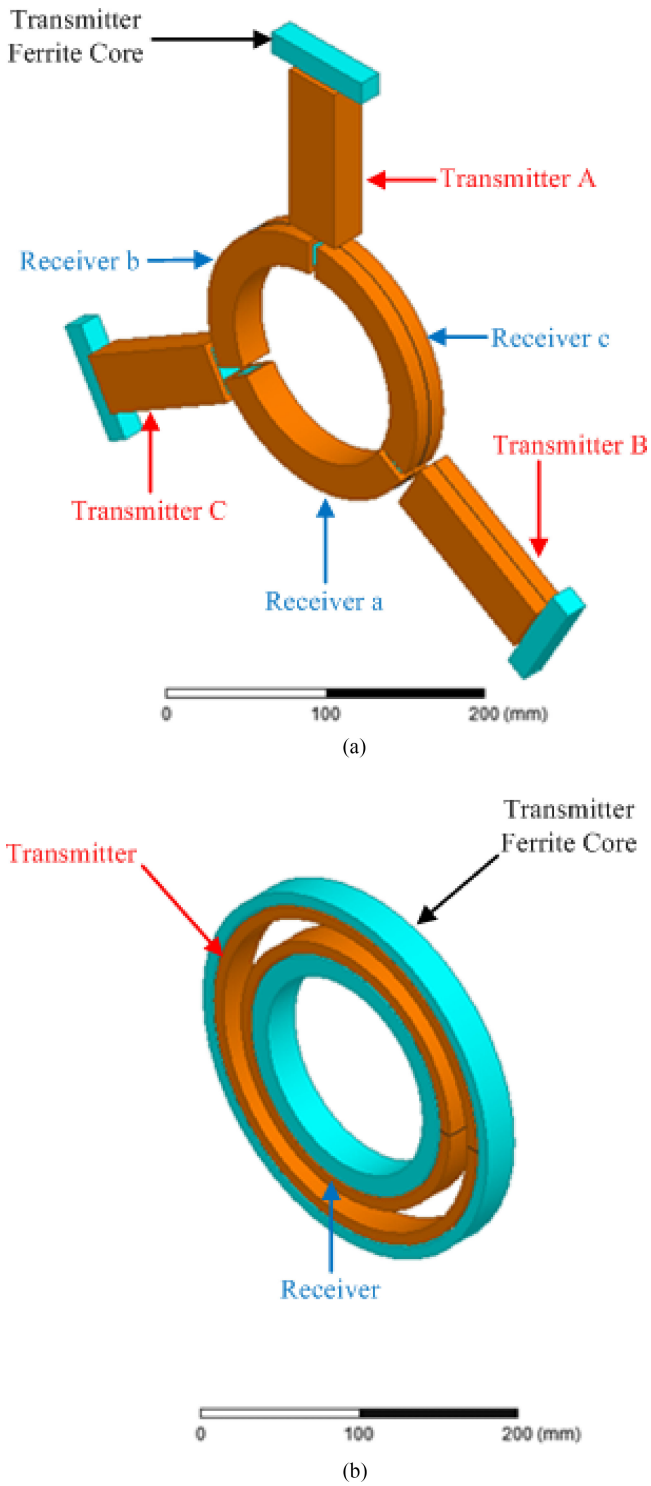

Fig. 1. Coil structures in simulation: (a) proposed three-phase coil structure and (b) coaxial coil structure.

in designing a wireless charging system is to design a coil structure to have few adverse effects on the shape of the AUV's hull and the existing electronics devices within the AUV.

Nowadays, composite materials with isolation properties, such as fiberglass, are commonly used as the hull material for AUVs [18], which makes it possible to install the receiver in the AUV without adversely affecting the shape of the AUV's hull. In this paper, a new three-phase coil structure consisting of three identical transmitters and three identical receivers, as shown in Fig. 1(a), is proposed. To further show the advantages of the proposed three-phase coil structure over a conventional coaxial coil structure shown in Fig. 1(b), magnetic field studies have been conducted for both coil structures. Through ANSYS MAXWELL simulations, it is demonstrated that the magnetic field generated by the proposed coil structure is concentrated in the coil structure instead of elsewhere within the AUV's hull. As a result, interference to the existing electronics devices in the AUV will be less, and more space will, thus, be available within the AUV for instrumentation. The proposed circuit is further analyzed and compensation methods to achieve resonance are introduced. Subsequently, a 1.0 kW three-phase wireless charging system with 92.41% dc–dc efficiency is designed and tested to validate the proposed concept.

II. Coil Design

Coil design is important in all wireless power transfer systems, as the geometries and properties of the coils ultimately set limits on power transfer capabilities and power transfer efficiency. In addition, coil design directly determines field patterns, which are important to manage so as to not adversely affect the existing electronics devices in an AUV. This is especially important, since the size of an AUV is compact and space within it is quite limited. As a result, it is desired to concentrate magnetic fields generated by the coil structure within the coil structure itself, and outside of the interior of the AUV's hull so that the existing electronics devices in the AUV are not adversely affected. Fig. 1(a) shows the proposed coil structure, which consists of three identical transmitters and three identical receivers. The excitation currents in all transmitters have the same magnitude and frequency, but are 120° out of phase. The magnetic flux excited by the current in one transmitter passes through the AUV's hull, couples with its two adjacent receivers, and goes back to that transmitter. In order to demonstrate the advantages of the proposed coil structure over the conventional coaxial one, a three-dimensional (3-D) finite-element analysis (FEA) tool (ANSYS MAXWELL) is employed and magnetic field studies are conducted in both the three-phase and coaxial coil structures presented in this section. Additionally, the materials used in two wireless charging systems with the two respective coil structures are compared. Furthermore, the parameters of the proposed coil structure in both seawater condition and ambient air condition are investigated.

A. Coil Structures Design

A 3-D overview and a cross-sectional front view of the simulation model of the proposed coil structure are shown in Fig. 2. In this simulation setup, the transmitters with the primary capacitors are packaged with water-resistant materials and immersed in seawater, and the receivers with the secondary capacitors are encapsulated in the AUV's hull. The hull, whose outer diameter is 200 mm, is made up of fiberglass and filled with air. The simulation model for the coaxial coil structure has the same

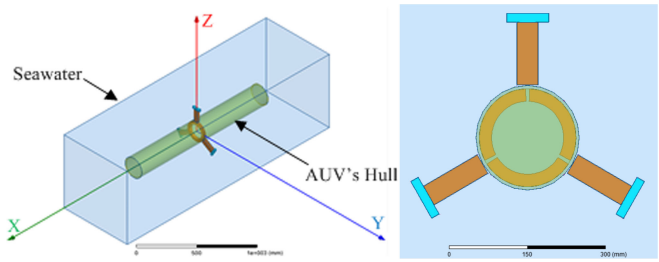

Fig. 2. (a) Overview and (b) front view of MAXWELL simulation model for the proposed coil structure.

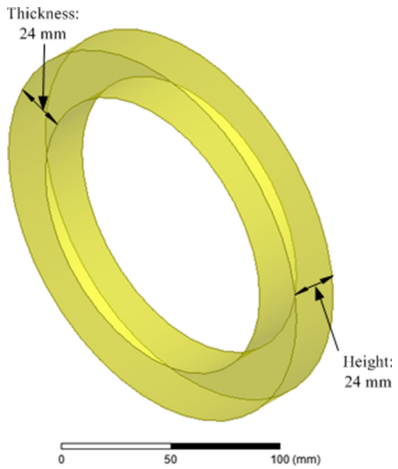

Fig. 3. Hollow cylinder for receivers.

dimensions of the seawater and AUV's hull; the only difference between the two models is the coil structure.

Due to the compactness of the AUV, the volume of any coil structure is important. In this study, 1.0 kW power is required to be transferred by both wireless charging systems to facilitate rapid charging. The frequency is assigned to be 465 kHz, which makes the system compact and ensures sufficient power can be transferred to the load. In order to make a fair comparison, the receivers of both coil structures are set to occupy the same volume. As shown in Fig. 3, they are fixed within dimensions of a hollow cylinder with an outer radius of 94 mm, an inner radius of 70 mm, and a height of 24 mm.

Though the geometries of the transmitters in the two coil structures are different, the volumes are designed approximately the same at 350 000 mm^3. Fig. 4 gives the design variables: (a) primary coil length and secondary coil angle for the proposed coil structure and (b) primary coil width and secondary coil width for the coaxial coil structure.

Variant mutual inductances can be achieved by sweeping the design variables within the limitations of the coil structure dimensions. The mutual inductance of a coil structure determines its capability of transferring power, and for a 1.0 kW design, a mutual inductance value of 7 μH is desired at the frequencies of interest. Therefore, the sets of design variables to achieve 7 μH mutual inductances are selected for both two coil structures. The simulated parameters are given in Table I. Specifically, the mutual inductance in the proposed coil structure refers to the mutual inductance between one transmitter and one of its adjacent receivers.

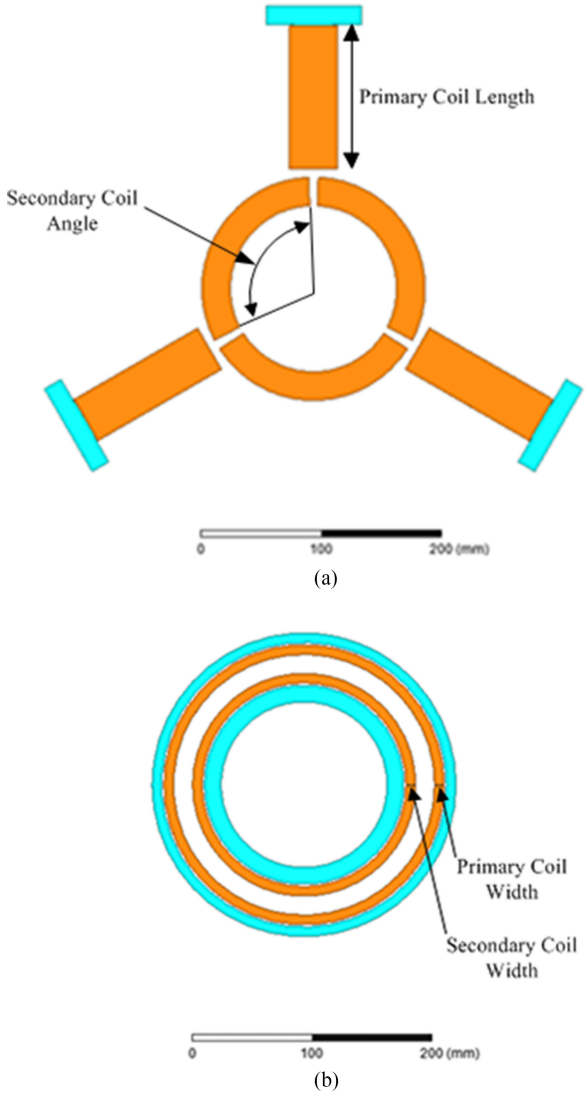

Fig. 4. Design variables in (a) proposed coil structure and (b) coaxial coil structure.

TABLE I
SIMULATION RESULTS

Parameters	Proposed Coil	Coaxial Coil
Transmitter's Self-inductance L_t	68.86 μH	13.09 μH
Receiver's Self-inductance L_r	33.67 μH	14.88 μH
Coupling Coefficient k_{tr} between L_t and L_r	0.1385	0.5130
Mutual Inductance M_{tr} between L_t and L_r	6.67 μH	7.16 μH

Simulation studies on rotational misalignment are also conducted for the two coil structures. Fig. 5(a) shows the rotational angle for the three-phase coil structure, noting that the relative separation between the transmitting coils is fixed during rotation. Fig. 5(b) shows the coaxial model. The variations in mutual inductance for both models are shown in Fig. 5(c). As the rotational angle increases from 0° to 25°, the mutual induc-

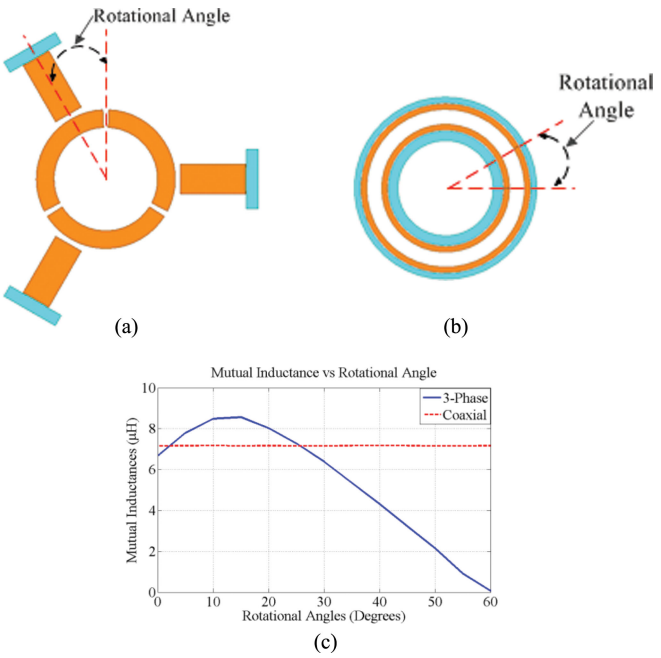

Fig. 5. (a) Rotational angle in the proposed coil structure. (b) Rotational angle in coaxial coil structure. (c) Mutual inductances variation with rotational angles.

tance in the proposed three-phase coil structure is competitive or exceeds that of the coaxial coil structure. However, as the rotational angle increases from 25° to 60°, the mutual inductance in the proposed coil structure drops dramatically and ends at zero, while the mutual inductance in the coaxial coil structure remains constant. Therefore, the coaxial coil structure has more stable performance on rotational misalignment than the proposed coil structure. However, rotational misalignment in the proposed coil structure can be eliminated by employing an advanced mechanical positioning system since three transmitters are separate and flexible to move. Therefore, the following analysis and experiment are conducted in full aligned condition.

B. Magnetic Field Studies

The main advantage of the proposed coil structure over the conventional coaxial coil structure is that the generated magnetic field is concentrated within the coil structure itself, which has fewer adverse effects on the existing electronics devices in the AUV. In order to study and compare the magnetic fields, both coil structures are required to transfer 1.0 kW power with the same charging current, which is the root mean square (rms) value of the alternating current before the rectifier and fixed at 10 A. A series–series compensation topology is applied due to its simplicity, constant-current principle, and ability to deliver high power at reasonable voltage levels [19], [20]. The excitation currents and the turn numbers for transmitters and receivers are given in Table II, where I_t is the transmitter's current, I_r is the receiver's current, and $\omega M_{tr} I_t$ is the equivalent voltage on the receiver's side induced by the transmitter's current. All the voltage and current values in Table II are rms values. Furthermore, the ampere-turns in the receivers of the two coil structures are kept the same.

TABLE II
EXCITATIONS IN SIMULATION

Parameters	Proposed Coil	Coaxial Coil
Transmitter's Current I_t	5.13 A	4.78 A
Receiver's Current I_r	3.33 A	10 A
Turn Number of Transmitter's Coil	22	5
Turn Number of Receiver's Coil	18	6
Induced Voltage $\omega M_{tr} I_t$	100 V	100 V
Total Charging Current	10 A	10 A
Power	1.0 kW	1.0 kW

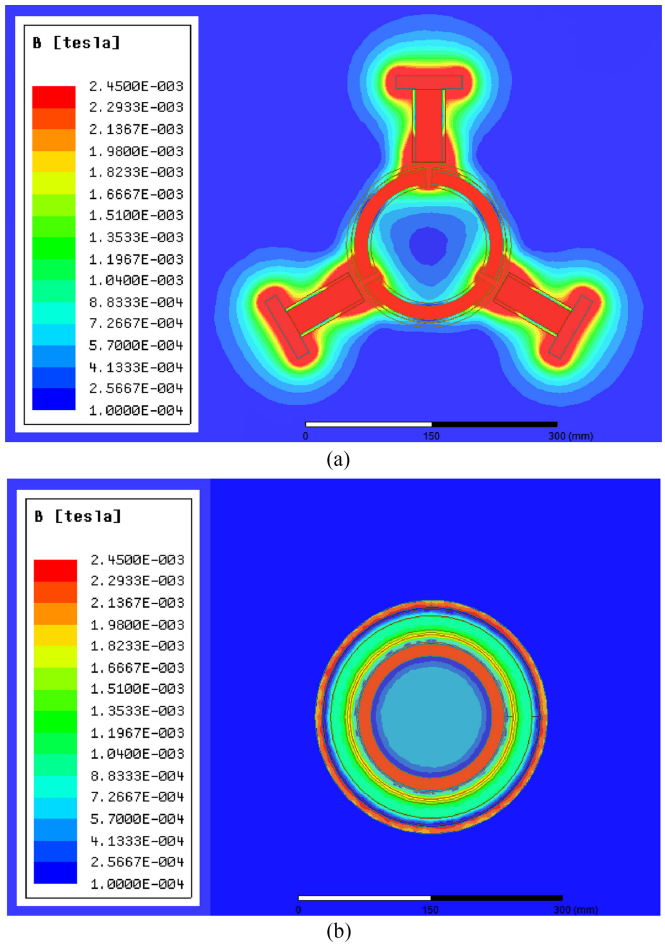

Fig. 6. Magnetic flux densities in *YZ* plane: (a) proposed coil structure and (b) coaxial coil structure.

The two coil structures were implemented in ANSYS MAXWELL, and simulation results of the magnetic flux densities of the two coil structures in *YZ*, *ZX*, and *XY* plane are shown in Figs. 6–8 respectively. The scale bars in the figures are all the same: 2.45×10^{-3} T at maximum and 1×10^{-4} T at minimum. Here, the light stripes in Figs. 7 and 8 stand for the AUV's position in simulation. Both the proposed coil structure and the coaxial coil structure perform fairly well in the *YZ* plane. The generated magnetic field of the proposed coil structure in the AUV is stronger around the receivers and weaker in the center, while the generated magnetic field of the coaxial structure is weaker around its receiver and stronger in the center.

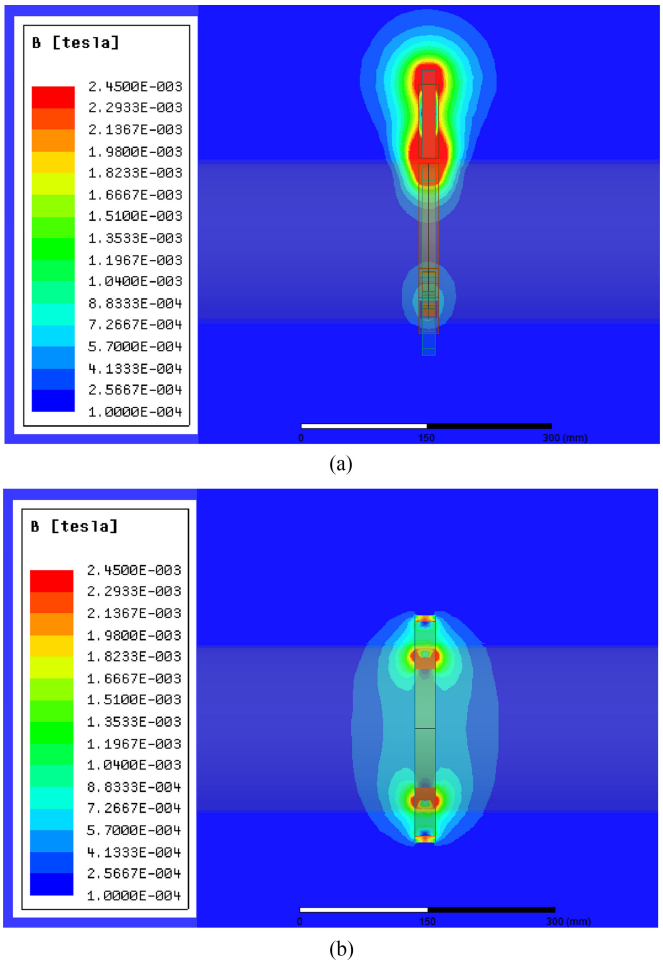

Fig. 7. Magnetic flux densities in *ZX* plane: (a) proposed coil structure and (b) coaxial coil structure.

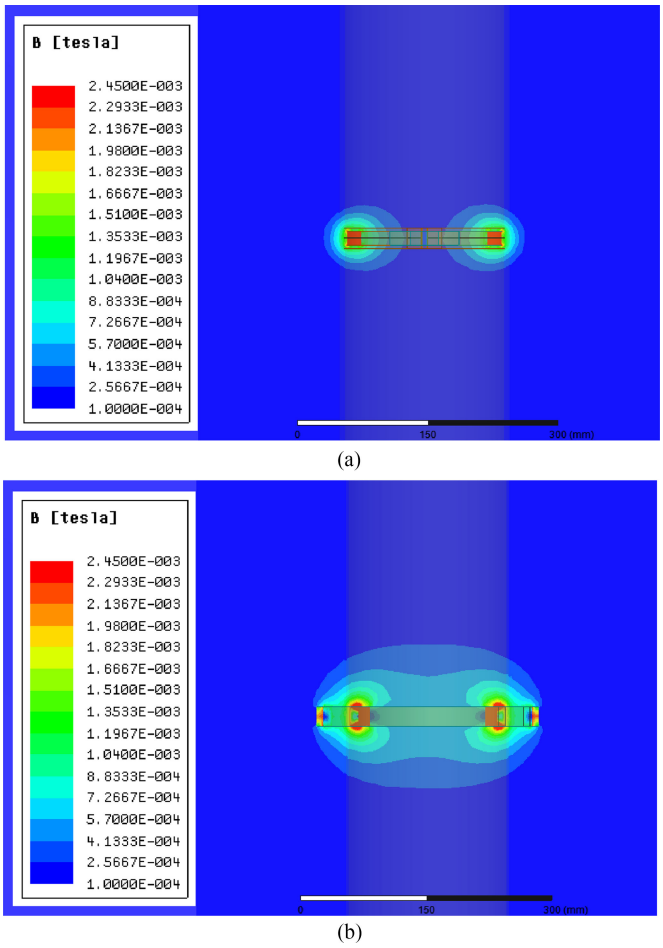

Fig. 8. Magnetic flux densities in *XY* plane: (a) proposed coil structure and (b) coaxial coil structure.

Even though a ferrite core is employed at receiver's side in the coaxial coil structure, a certain amount of magnetic fluxes still exist in the center. Moreover, Figs. 7(b) and 8(b) indicate the generated magnetic field of the coaxial coil structure is more divergent in *ZX* and *XY* plane. Instead, Figs. 7(a) and 8(a) show the proposed coil structure gives outstanding performance in *ZX* and *XY* plane. The generated magnetic field is more concentrated in the coil structure rather than disperses from it. As a result, the existing electronics devices are less affected, meaning that they can be installed closer to the coil structure and more space will be available in the AUV.

C. Materials Comparison

To further compare the two coil structures, materials used in building the two wireless charging systems are analyzed. The comparison is focused on materials used in three stages: the inverter stage, the rectifier stage, and the resonant tank stage. In the inverter and rectifier stages, the materials used in the proposed three-phase system are three times of those in the conventional single-phase system. For example, if full-bridge inverters and full-bridge rectifiers are applied for power conversion, three inverters consisting of 12 MOSFETs and three rectifiers with 12 diodes will be employed in the proposed three-phase system while only one inverter with four MOSFETs and one rectifier with four diodes will be used in the conventional single-phase system. The conventional single-phase system with the coaxial coil structure is more cost beneficial in the inverter and rectifier stages. The resonant tank is mainly constituted by the coil structure and the series resonant capacitors. A total of 202 321 mm^3 of copper and 310 724 mm^3 of ferrite are used in the proposed coil structure while the volumes of copper and ferrite in the coaxial coil structure are 229 211 and 319 387 mm^3. In the proposed coil structure, three transmitter's capacitors, which are in series with transmitter's coils, and three receiver's capacitors, which are in series with receiver's coils, are employed. The voltage across each transmitter's capacitor is 1.032 kV and the current passing through it is 5.13 A. The voltage across each receiver's capacitor is 319.7 V and the current passing through it is 3.33 A. In the coaxial coil structure, one transmitter's capacitor and one receiver's capacitor are selected. Each transmitter's capacitor is required to withstand a voltage of 182.8 V and a current of 4.78 A. Each receiver's capacitor is capable of bearing a voltage of 434.8 V and a current of 10 A. All the voltage and current values are in rms and they are calculated by equations in Section III.

TABLE III
MATERIALS COMPARISON

Items	Proposed Coil	Coaxial Coil
Number of Inverters	3	1
Number of Rectifiers	3	1
Copper	202 321 mm^3	229 211 mm^3
Ferrite	310 724 mm^3	319 387 mm^3
Number of Capacitors	6	2
VA rating of TX's Capacitor	5.295 kVA	0.874 kVA
VA rating of RX's Capacitor	1.065 kVA	4.347 kVA

TABLE IV
PARAMETERS COMPARISON

Parameters	Seawater	Ambient Air	Error
L_t	68.86 μH	69.56 μH	1.02%
L_r	33.67 μH	33.98 μH	0.92%
k_{tr}	0.1385	0.1393	0.58%
k_{rr}	0.2404	0.2399	0.21%
k_{tt}	0.0256	0.0264	3.13%
k_{tr0}	≈0	≈0	0%

The comparison results on materials are summarized in Table III. The wireless charging system with the coaxial coil structure uses fewer inverters and rectifiers while the wireless charging system with the proposed coil structure uses a smaller amount of copper and ferrite materials. The voltampere (VA) ratings of the capacitors range from several hundred VA to several thousand VA; however, fewer capacitors are applied in the wireless charging system with coaxial coil structure. Thus, despite some disadvantages in copper and ferrite materials, it is estimated that the conventional single-phase coaxial wireless charging system is more cost beneficial from a materials point of view.

D. Investigation on Parameters of the Proposed Coil Structure in Two Conditions

The conductivity of seawater is only 4 S/m and its relative magnetic permeability is very close to 1. Thus, to the first order the seawater can be considered as air at the frequencies of interest. Specifically, the magnetic fields generated by the coil structure in seawater will be approximately the same with that in air, and the eddy current loss in seawater will be very small. To validate this assumption, a simulation model with neither seawater nor the AUV's hull but only the ambient air is built and the simulated results are contrasted to those with seawater and the AUV's hull. The parameters are illustrated in Fig. 9 and compared in Table IV, where L_t is transmitter's coil inductance, L_r is the receiver's coil inductance, k_{tr} is the coupling coefficient between one transmitter and one of its two adjacent receivers, k_{tr0} is the coupling coefficient between one transmitter and its away receiver, k_{tt} is the coupling coefficient between two transmitters, and k_{rr} is the coupling coefficient between two receivers. The differences in coil parameters between the original model and ambient air model are small. Moreover, a simulation on the magnetic field generated by the proposed coil structure in the ambient air condition is performed and simulation results demonstrate that the generated magnetic field is the same in two conditions. In order to simplify the analysis and experiment, the seawater and the AUV's hull are ignored in later sections.

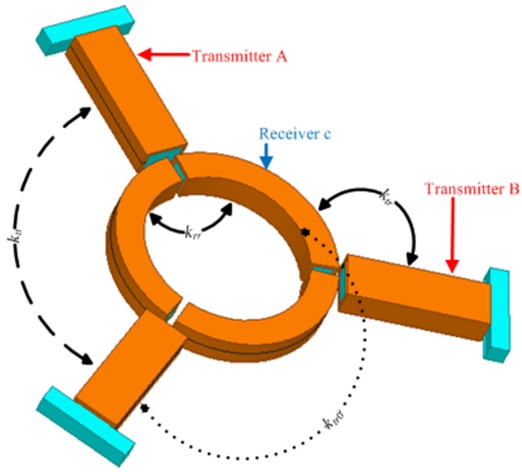

Fig. 9. Instructions on coil parameters.

III. CIRCUIT ANALYSIS

Analysis is focused on the circuit from dc power supply to dc electronic load. Full-bridge inverters are chosen to convert dc power to high-frequency ac power. The ac power flows into the transmitter's resonant tank formed by the transmitter's compensation capacitor C_t in series with the transmitter's coil L_t. It resonates in the transmitter's resonant tank at a single resonant frequency and wirelessly transfers to the receiver's resonant tank through the mutual inductance between the transmitter's coil and the receiver's coil. The receiver's resonant tank has the same resonant frequency with the transmitter's resonant tank and is constituted by the receiver's compensation capacitor C_r in series with the receiver's coil L_r. The high-frequency resonating ac power gets rectified to dc power by full-bridge rectifiers. In the three-phase wireless charging system, three inverters and three rectifiers are employed. The three transmitters are named as A, B, and C. The receiver away from transmitter A is receiver a, and likewise for B and C (b and c). For simplicity, only one inverter at transmitter A and one rectifier at receiver c are shown in Fig. 10, where U_{in} is the dc voltage of dc power supply, u_A is the ac input voltage of transmitter A's resonant tank, and R_L is the resistance of the dc electronic load. Since a series–series compensation topology is selected, the circuit behaves like a constant voltage (CV) source. However, if the input voltage to the inverter is a constant, then its output current is also a constant. Therefore, based on [21], the ac input voltage u_A and the equivalent resistance R_{eq} of load resistance R_L at the rectifier's input side can be expressed as

$$u_A = \frac{2\sqrt{2}}{\pi} U_{in} \angle 0^\circ \tag{1}$$

$$R_{eq} = \frac{8}{\pi^2} R_L. \tag{2}$$

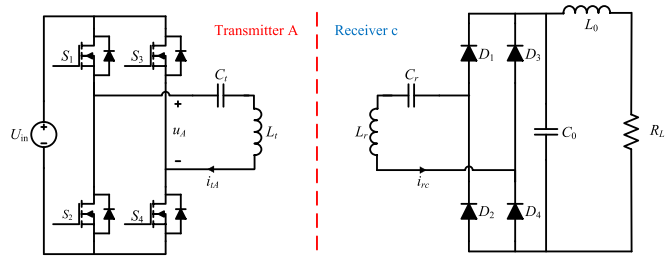

Fig. 10. Full-bridge inverter at transmitter A and full-bridge rectifier at receiver c.

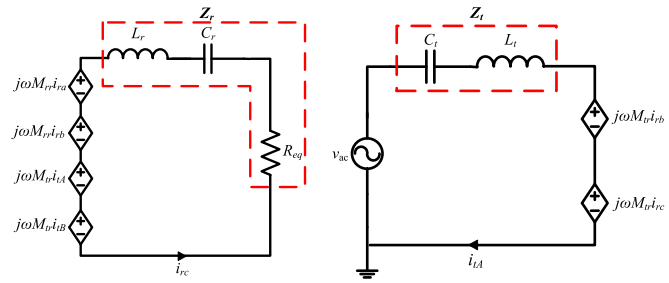

Fig. 11. Equivalent mutual inductance models for (a) receiver c and (b) transmitter A.

Three full-bridge inverters convert the dc input voltage to three ac voltages with the same magnitude and frequency, yet at 120° out of phase. Since the initial phase angle of u_A is assigned to be 0°, the initial phase angles of transmitter B's ac input voltage u_B and transmitter C's input voltage u_C are 120° and 240°. Resonance is achieved on both transmitter's side and receiver's side. Therefore, the current in each transmitter is in phase with the respective input ac voltage and the current in each receiver is in phase with the respective induced voltage. The transmitter's currents i_{tA}, i_{tB}, and i_{tC} have the same magnitude I_t and initial phase angles of 0°, 120°, and 240°, respectively. The induced voltages $j\omega M_{tr}i_{tA}$, $j\omega M_{tr}i_{tB}$, and $j\omega M_{tr}i_{tC}$, from transmitter's side to receiver's side, have initial phase angles of 90°, 210°, and 330°, respectively. Based on the simulation results in Section II, k_{tt} and k_{tr0} are considerably small. The coupling effect between each two transmitters and the coupling effect between each transmitter and its away receiver can be neglected in analysis. The coupling effect between each transmitter and its adjacent receivers and the coupling effect between each two receivers are dominant. The equivalent mutual inductance models for receiver c and transmitter A are shown in Fig. 11, where M_{rr} is the mutual inductance between two receivers. Here, the full-bridge inverter and rectifier are omitted. Furthermore, the equivalent series resistance of all the capacitors and inductors are ignored in analysis. As can be seen in Fig 11(a), the initial phase angle of the receiver c's current i_{rc} is determined by $j\omega M_{tr}i_{tA}$ and $j\omega M_{tr}i_{tB}$. According to the triangle rule, the initial phase angle of i_{rc} is 150°. Similarly, the initial phase angle of the receiver a's current i_{ra} and the receiver b's current i_{rb} are 270° and 30°. Moreover, i_{ra}, i_{rb}, and i_{rc} have the same magnitude I_r.

In the resonance condition, the capacitor C_r on receiver's side is required to compensate the receiver coil's self-inductance as well as the equivalent inductances caused by two induced voltages from the other two receivers. The capacitor C_t on transmitter's side only compensates the transmitter coil's self-inductance since the reflected impedances Z_{refl} from the receiver's side to the transmitter's side are purely resistive.

TABLE V
DIMENSIONAL PARAMETERS

Parameters	Values
I core size	80 mm * 32 mm * 16 mm
Wing core size	80 mm * 16 mm * 16 mm
Number of turns in transmitter's coil L_t	20
Number of turns in receiver's coil L_r	16
Air Gap	21 mm
Wire diameter	4 mm

$$\omega L_r - \frac{1}{\omega C_r} + \frac{\omega M_{rr} i_{ra} + \omega M_{rr} i_{rb}}{i_{rc}} = 0 \tag{3}$$

$$\mathrm{Im}\,(Z_{refl}) = \mathrm{Im}\left(\frac{j\omega M_{tr} i_{rb} + j\omega M_{tr} i_{rc}}{i_{ta}}\right) = 0 \tag{4}$$

$$\omega L_t - \frac{1}{\omega C_t} = 0 \tag{5}$$

where ω is angular resonant frequency. The impedances Z_r and Z_t are defined in Fig. 11 and written as

$$Z_r = j\omega L_r + \frac{1}{j\omega C_r} + R_{eq} \tag{6}$$

$$Z_t = j\omega L_t + \frac{1}{j\omega C_t}. \tag{7}$$

Kirchhoff's voltage law is applied and six voltage equations are derived as

$$\begin{bmatrix} u_A \\ u_B \\ u_C \\ 0 \\ 0 \\ 0 \end{bmatrix} = \begin{bmatrix} Z_t & 0 & 0 & 0 & j\omega M_{tr} & j\omega M_{tr} \\ 0 & Z_t & 0 & j\omega M_{tr} & 0 & j\omega M_{tr} \\ 0 & 0 & Z_t & j\omega M_{tr} & j\omega M_{tr} & 0 \\ 0 & j\omega M_{tr} & j\omega M_{tr} & Z_r & j\omega M_{rr} & j\omega M_{rr} \\ j\omega M_{tr} & 0 & j\omega M_{tr} & j\omega M_{rr} & Z_r & j\omega M_{rr} \\ j\omega M_{tr} & j\omega M_{tr} & 0 & j\omega M_{rr} & j\omega M_{rr} & Z_r \end{bmatrix} \cdot \begin{bmatrix} i_{ta} \\ i_{tb} \\ i_{tc} \\ i_{ra} \\ i_{rb} \\ i_{rc} \end{bmatrix}. \tag{8}$$

By substituting (3), (5), (6) and (7) into (8), six currents can be solved as

$$\begin{bmatrix} i_{tA} \\ i_{tB} \\ i_{tC} \\ i_{ra} \\ i_{rb} \\ i_{rc} \end{bmatrix} = \begin{bmatrix} \frac{u_A R_{eq}}{\omega^2 M_{tr}^2} & \frac{u_B R_{eq}}{\omega^2 M_{tr}^2} & \frac{u_C R_{eq}}{\omega^2 M_{tr}^2} & j\frac{u_a}{\omega M_{tr}} & j\frac{u_b}{\omega M_{tr}} & j\frac{u_c}{\omega M_{tr}} \end{bmatrix}^T. \tag{9}$$

TABLE VI
COMPARISON BETWEEN SIMULATED AND MEASURED RESULTS

Para.	Sim.	Mea.	Para.	Sim.	Mea.	Para.	Sim.	Mea.	Para.	Sim.	Mea.
L_A	56.29 μH	56.87 μH	M_{Ab}	6.644 μH	6.815 μH	M_{AB}	2.333 μH	2.893 μH	M_{Aa}	0.0005 μH	0.005 μH
L_B	56.26 μH	56.96 μH	M_{Ac}	6.641 μH	6.685 μH	M_{BC}	2.334 μH	2.540 μH	M_{Bb}	0.001 μH	0.258 μH
L_C	56.30 μH	56.51 μH	M_{Ba}	6.640 μH	6.803 μH	M_{CA}	2.329 μH	2.663 μH	M_{Cc}	0.002 μH	0.510 μH
L_a	31.34 μH	31.64 μH	M_{Bc}	6.639 μH	6.610 μH	M_{ab}	4.433 μH	3.450 μH			
L_b	31.34 μH	31.70 μH	M_{Ca}	6.636 μH	6.610 μH	M_{bc}	4.434 μH	4.570 μH			
L_c	31.28 μH	31.40 μH	M_{Cb}	6.641 μH	6.663 μH	M_{ca}	4.426 μH	3.538 μH			

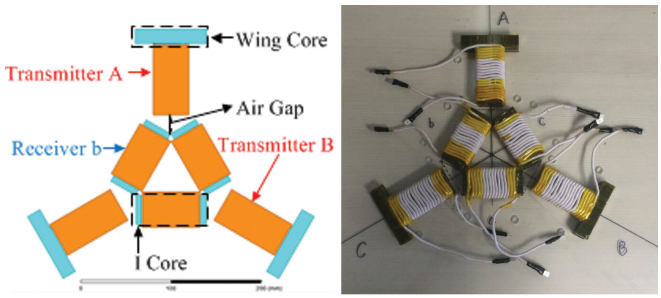

Fig. 12. (a) Simulation and (b) experimental models of the proposed coil structure in Section IV.

The real power transferred from the transmitter's side to the receiver's side is

$$P_{\text{real}} = \text{Re}(u_A \cdot i_{\text{tA}}^* + u_B \cdot i_{\text{tB}}^* + u_C \cdot i_{\text{tC}}^*) = \frac{3U_A^2 R_{\text{eq}}}{\omega^2 M_{\text{tr}}^2}. \quad (10)$$

Combining (1), (2) with (9), the power equation from dc power supply to dc electronic load is

$$P = \frac{192 \cdot U_{\text{in}}^2 R_{\text{L}}}{\pi^4 \omega^2 M_{\text{tr}}^2}. \quad (11)$$

IV. EXPERIMENTAL RESULTS

A three-phase wireless charging system is designed and tested to verify the proposed concept and compensation method. As indicated in Section II, the seawater and the AUV's hull are reasonably ignored: unless otherwise specified, both simulations and experiments in this section are conducted in ambient air conditions. Unfortunately, it is extremely difficult to find appropriate arc-shape ferrite cores off-the-shelf. Thus, straight ferrite bars are employed for the receivers for convenience. Moreover, the available ferrite bars are smaller than the arc-shape ferrite cores in the simulation of Section II. Therefore, the turn numbers are slightly different from those in the simulation of Section II. However, the mutual inductance values in both sections are kept nearly the same. The resonant frequency is set to be 465 kHz. The dimensional parameters of the coil structure are given in Table V and depicted in Fig. 12(a). The coils are color coded in orange, and the cores in blue. In this experiment, 3000-strand AWG-46 litz wires and 3C95 ferrite from Ferroxcube are used to build the coil structure, which are shown in Fig. 12(b).

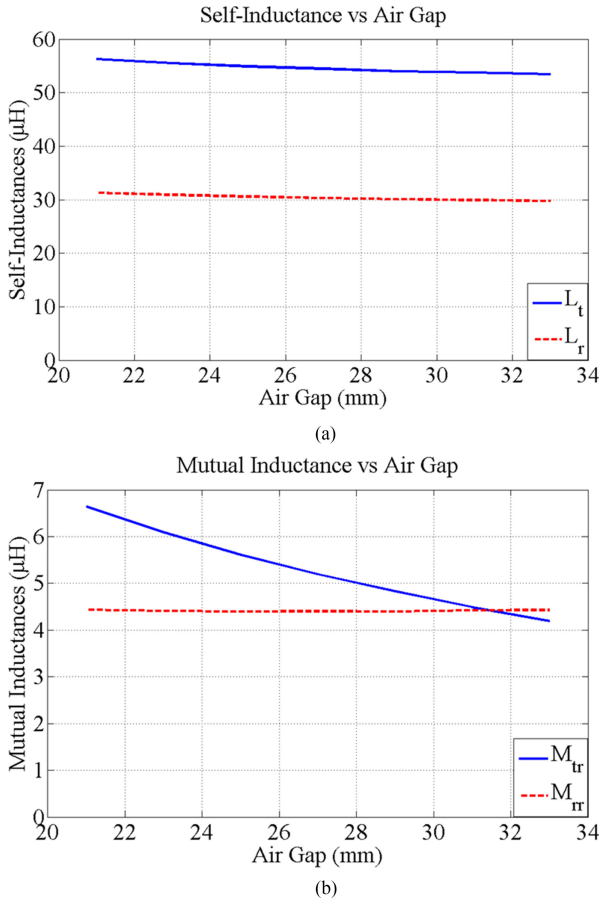

Fig. 13. (a) Self-inductances and (b) Mutual inductances with air gap variation.

A comparison of the simulated and measured results is drawn in Table VI, where L is the self-inductance and M is the mutual inductance. At the positions of subscripts, uppercase letters A, B, and C accordingly stand for transmitters A, B, and C while lowercase letters a, b, and c successively represent receivers a, b, and c. For example, L_{A} is the self-inductance of transmitter A and M_{Bc} is the mutual inductance between transmitter B and receiver c. As indicated by Table VI, the measured self-inductances L and mutual inductances M_{tr} between one transmitter and one of its adjacent receivers closely match the simulated ones, which are desired since the three-phase wireless charging system relies on M_{tr} to transfer power. The measured mutual inductances M_{tt} and M_{tr0} show good agreement with the simulations: the maximum difference among them is only 0.66 μH. However, the differ-

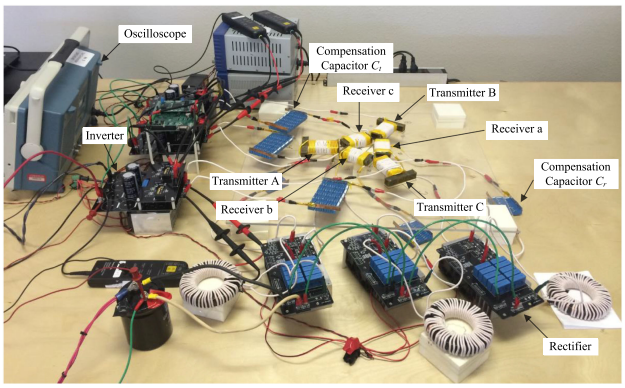

Fig. 14. Experimental setup.

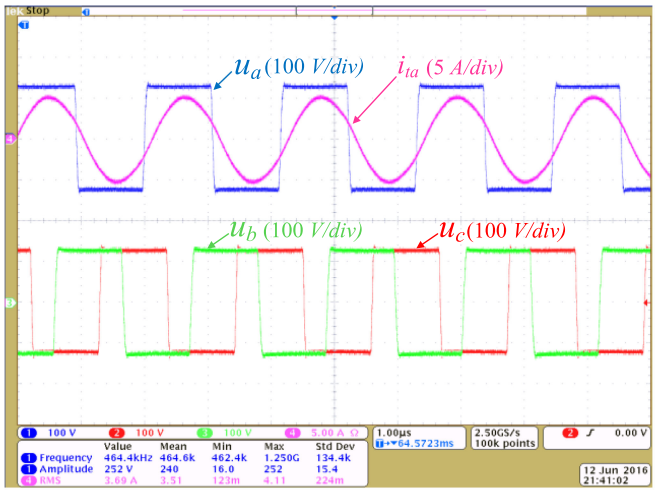

Fig. 15. Waveforms at $P_{out} = 1.0\,\text{kW}$ and $\text{CR} = 12\,\Omega$.

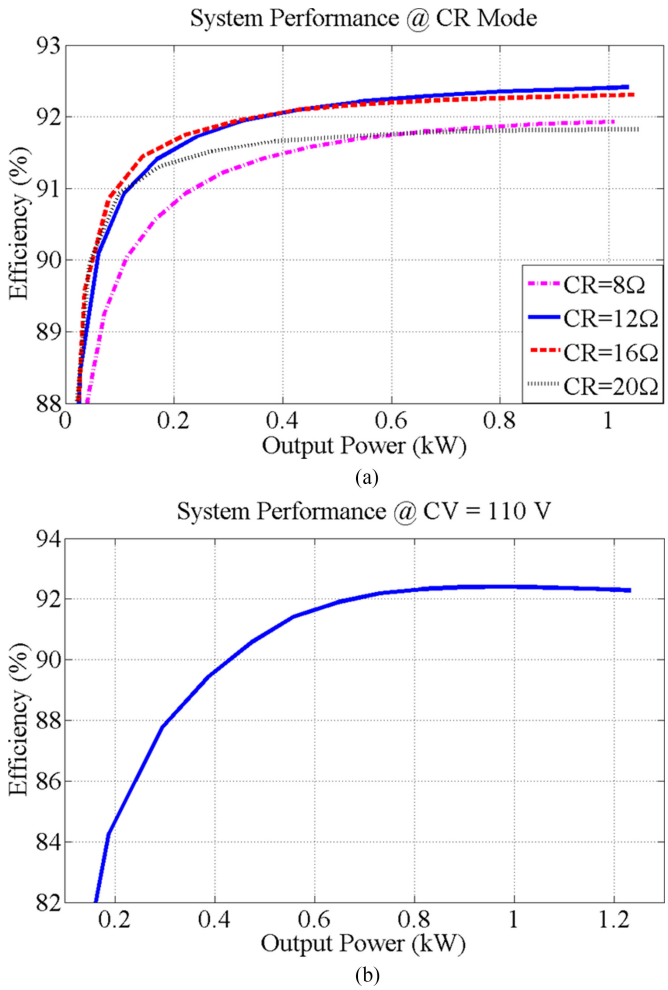

Fig. 16. System performance at (a) CR mode and (b) CV mode in ambient air condition.

ence between the simulated and measured mutual inductances M_{rr} cannot be further ignored for an accurate experiment since its maximum value is approximately 1 μH. Moreover, it is difficult to fix this problem manually because the receivers are close to each other and parameters are correlated. A slight misalignment may lead to an obvious change in all self-inductances and mutual inductances. In order to minimize the effect, the arithmetic mean value of each two mutual inductances is selected as M_{rr} and applied in (3) of Section III to calculate the respective compensation capacitor values on receiver's side. For example, in the calculation of the compensation capacitor C_r at receiver c, the arithmetic mean value of M_{ca} and M_{bc} are determined and substituted into M_{rr} in (3). The compensation capacitor values on transmitter's side are determined based on (5).

Simulations on air gap variation are conducted and the results are shown in Fig. 13. The transmitter's and receiver's self-inductances L_t, L_r, and the mutual inductance M_{rr} are kept almost the same as air gap varies. Therefore, based on (3)–(5), the resonance remains. However, the mutual inductance M_{tr} decreases. Since power transfer relies on mutual inductance, the input voltage is required to increase with a larger air gap if the same output power is desired for dynamic charging applications.

The three-phase wireless charging system is built as shown in Fig. 14. Since the purpose of the experiment is to verify the proposed concept, three full-bridge inverters and three full-bridge rectifiers are selected for power conversion due to the convenience in lab. However, a three-phase inverter and a three-phase rectifier, which have competitive volumes with the single-phase ones, will be designed and chosen for practical applications. Experiments are conducted from dc power source to dc electronic load. Constant resistance (CR) mode and CV mode of the dc electronic load are chosen to emulate a rechargeable battery. In this paper, the selected CRs and voltage are 8 Ω, 12 Ω, 16 Ω, 20 Ω, and 110 V. Voltage and current waveforms when output power is 1.0 kW and resistance is 12 Ω are given in Fig. 15. The input current i_{tA} in transmitter A lags its input voltage u_A by 18°, which ensures that the current is sufficient to charge the parasitic capacitors of the MOSFETs. Zero-voltage switching is achieved and the switching losses and noises are reduced.

Experimental results on system power and efficiency in ambient air condition are shown in Fig. 16. The three-phase wireless charging system is able to deliver 1.0 kW from transmitters to receivers. As the resistance varies in Fig. 16(a), the efficiency is maximized at 92.41%. Furthermore, it is demonstrated in Fig. 16(b) that the system transfers 1.0 kW at dc–dc efficiency of 92.41% when the output voltage is constant at 110 V. Exper-

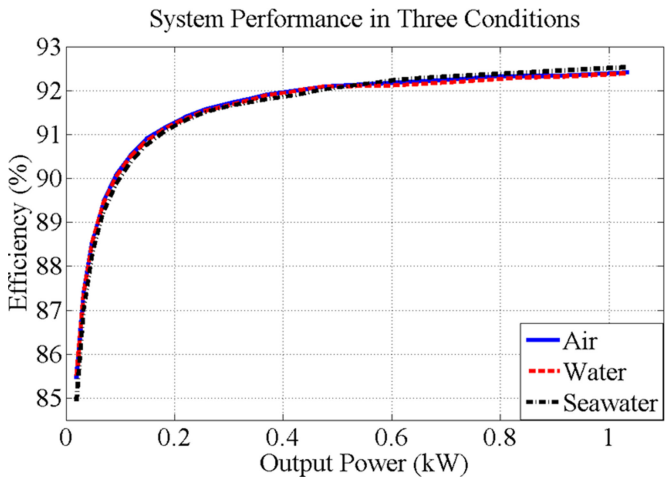

Fig. 17. System performance in three conditions.

iments under water and seawater conditions, in which multiple bottles of water or seawater are placed along the coils, are also separately conducted. The differences of the results among ambient air, water, and seawater conditions are very minor, which are shown in Fig. 17. The proposed concept is, thus, verified by experiment.

V. Conclusion

In this paper, a three-phase wireless charging system for lightweight AUVs is proposed and analyzed. Three dimensional (3-D) FEA simulations are performed to show the generated magnetic field by the proposed three-phase coil structure is concentrated in the coil structure and out of the AUV's hull, which has fewer adverse effects on the existing electronics devices in the AUV. Circuit analysis and compensation methods to achieve resonance are presented. A three-phase wireless charging system is designed and built for experiment. It is demonstrated that the system successfully delivers 1.0 kW with a dc–dc efficiency of 92.41% at 465 kHz, which verifies the proposed design.

Our future work includes 1) downsizing the power electronics circuits and minimizing the number of transistors used in experiment and 2) the effects on marine life at the frequency of interests.

References

[1] H. Hertz, *Dictionary of Scientific Biography*, vol. VI. New York, NY, USA: Scribner, 1970, pp. 340–349.
[2] N. Tesla, "Apparatus for transmitting electrical energy," U.S. Patent 119732 A, Dec. 1914.
[3] R. Wu, W. Li, H. Luo, J. K. O. Sin, and C. P. Yue, "Design and characterization of wireless power links for brain-machine interface applications," *IEEE Trans. Power Electron.*, vol. 29, no. 10, pp. 5462–5471, Jan. 2014.
[4] S. Raju, R. Wu, M. Chan, and C. P. Yue, "Modeling of mutual coupling between planar Inductors in wireless power applications," *IEEE Trans. Power Electron.*, vol. 29, no. 1, pp. 481–490, Jan. 2014.
[5] D. Ahn and P. P. Mercier, "Wireless power transfer with concurrent 200 kHz and 6.78 MHz operation in a single transmitter device," *IEEE Trans. Power Electron.*, vol. 31, no. 7, pp. 5018–5029, Jul. 2016.
[6] S. Y. Hui, "Planar wireless charging technology for portable electronic products and Qi," *Proc. IEEE*, vol. 101, no. 6, pp. 1290–1301, Jun. 2013.
[7] W. Li, H. Zhao, S. Li, J. Deng, T. Kan, and C. C. Mi, "Integrated LCC compensation topology for wireless charger in electric and plug-in electric vehicles," *IEEE Trans. Ind. Electron.*, vol. 62, no. 7, pp. 4215–4225, Dec. 2014.
[8] T. Kan, T. D. Nguyen, J. C. White, R. K. Malhan, and C. Mi, "A new integration method for an electric vehicle wireless charging system using LCC compensation topology," *IEEE Trans. Power Electron.*, vol. 32, no. 2, pp. 1638–1650, Feb. 2016.
[9] S. W. Li, and C. C. Mi, "Wireless power transfer for electric vehicle applications," *IEEE J. Emerg. Sel. Topics Power Electron*., vol. 3, no. 1, pp. 4–17, Mar. 2015.
[10] C. Park, S. Lee, S. Y. Jeong, G.-H. Cho, and C. T. Rim, "Uniform power I-type Inductive power transfer system with DQ-power supply rails for on-line electric vehicles," *IEEE Trans. Power Electron.*, vol. 30, no. 11, pp. 6446–6455, Nov. 2015.
[11] G. A. Covic and J. T. Boys, "Inductive power transfer," *Proc. IEEE*, vol. 101, no. 6, pp. 1276–1289, Jun. 2013.
[12] S. Y. R. Hui, W. Zhong, and C. K. Lee, "A critical review of recent progress in mid-range wireless power transfer," *IEEE Trans. Power Electron.*, vol. 29, no. 9, pp. 4500–4511, Sep. 2014.
[13] A. M. Bradley, M. D. Feezor, H. Singh, and F. Yates Sorrell, "Power systems for autonomous underwater vehicles," *IEEE J. Ocean. Eng.*, vol. 26, no. 4, pp. 526–538, Oct. 2001.
[14] M. D. Feezor, F. Y. Sorrell, and P. R. Blankinship, "An interface system for autonomous undersea vehicles," *IEEE J. Ocean. Eng.*, vol. 26, no. 4, pp. 522–525, Oct. 2001.
[15] T. McGinnis, C. P. Henze, and K. Conroy, "Inductive power system for autonomous underwater vehicles," in *Proc. OCEANS*, 2007, pp. 1–5.
[16] Z. Li, D. Li, L. Lin, and Y. Chen, "Design considerations for electromagnetic couplers in contactless power transmission systems for deep-sea applications," *J. Zhejiang Univ. Sci. C*, vol. 11, no. 10, pp. 824–834, Sep. 2010.
[17] J. Shi, D. Li, and C. Yang, "Design and analysis of an underwater inductive coupling power transfer system for autonomous underwater vehicle docking applications, " *J. Zhejiang Univ. Sci. C*, vol. 15, no. 1, pp. 51–62, Jan. 2014.
[18] C. T. Ross, "A conceptual design of an underwater vehicle," *Ocean Eng.*, vol. 33, no. 16, pp. 2087–2104, Nov. 2006.
[19] W. Zhang and C. C. Mi, "Compensation topologies of high-power wireless power transfer systems," *IEEE Trans. Veh. Technol.*, vol. 65, no. 6, pp. 4768–4778, Jun. 2016.
[20] P. P. Mercier and A. P. Chandrakasan, "Rapid wireless capacitor charging using a multi-tapped inductively-coupled secondary coil," *IEEE Trans. Circuits Syst. I, Reg. Papers*, vol. 60, no. 9, pp. 2263–2272, Sep. 2013.
[21] R. L. Steigerwald, "A comparison of half-bridge resonant converter topologies," *IEEE Trans. Power Electron.*, vol. 3, no. 2, pp. 174–182, Apr. 1998.

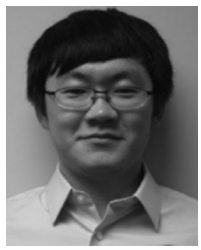

Tianze Kan (S'15) received the B.Eng. degree in electrical engineering and automation from Huazhong University of Science and Technology, Wuhan, China, in 2011 and the M.S. degree in electrical engineering from the University of Southern California, Los Angeles, CA, USA, in 2013. He is currently working toward the Ph.D. degree in electrical and computer engineering in the joint doctoral program between San Diego State University, San Diego, CA, USA, and the University of California San Diego, La Jolla, CA.

His research interests include power electronics and inductive-based wireless power transfer, especially on coil design and compensation topologies.

Ruikun Mai (M'14) received B.Sc. and Ph.D. degrees in electrical engineering from Southwest Jiaotong University, Chengdu, China, in 2004 and 2010, respectively.

He is currently an Associate Professor in the School of Electrical Engineering, Southwest Jiaotong University. His research interests include wireless power transfer and its application in railway systems, power system stability, and control

Patrick P. Mercier (S'04–M'12) received the B.Sc. degree in electrical and computer engineering from the University of Alberta, Edmonton, AB, Canada, in 2006, and the S.M. and Ph.D. degrees in electrical engineering and computer science from the Massachusetts Institute of Technology, Cambridge, MA, USA, in 2008 and 2012, respectively.

He is currently an Assistant Professor in Department of Electrical and Computer Engineering, University of California San Diego (UCSD), La Jolla, CA, USA, where he is also the Co-Director of the Center for Wearable Sensors. He was the co-editor of *Ultra-Low-Power Short Range Radios* (Springer, 2015) and *Power Management Integrated Circuits* (CRC Press, 2016). His research interests include the design of energy-efficient microsystems, focusing on the design of RF circuits, power converters, and sensor interfaces for miniaturized systems and biomedical applications.

Prof. Mercier was an Associate Editor of the IEEE TRANSACTIONS ON VERY LARGE SCALE INTEGRATION from 2015–2017. Since 2013, he has been an Associated Editor of the IEEE TRANSACTIONS ON BIOMEDICAL INTEGRATED CIRCUITS, and since 2017 has been a member of the ISSCC International Technical Program Committee (Technology Directions Sub-Committee) and CICC Technical Program Committee. He received the Natural Sciences and Engineering Council of Canada (NSERC) Julie Payette fellowship in 2006, the NSERC Postgraduate Scholarships in 2007 and 2009, an Intel Ph.D. Fellowship in 2009, the 2009 IEEE International Solid-State Circuits Conference (ISSCC) Jack Kilby Award for Outstanding Student Paper at ISSCC 2010, a Graduate Teaching Award in Electrical and Computer Engineering at UCSD in 2013, the Hellman Fellowship Award in 2014, the Beckman Young Investigator Award in 2015, the DARPA Young Faculty Award in 2015, the UCSD Academic Senate Distinguished Teaching Award in 2016, and the Biocom Catalyst Award in 2017.

Chunting Chris Mi (S'00–A'01–M'01–SM'03–F'12) received the B.S.E.E. and M.S.E.E. degrees in electrical engineering from Northwestern Polytechnical University, Xi'an, China, in 1985 and 1988, and the Ph.D. degree in electrical engineering from the University of Toronto, Toronto, ON, Canada, in 2001.

He is a Professor and a Chair of electrical and computer engineering and the Director of the Department of Energy funded Graduate Automotive Technology Education Center for Electric Drive Transportation, San Diego State University (SDSU), San Diego, CA, USA. Prior to joining SDSU, he was with the University of Michigan, Dearborn, MI, USA, from 2001 to 2015. From 2008 to 2011, he was the President and the Chief Technical Officer of 1Power Solutions, Inc. He is the Co-Founder of Gannon Motors and Controls LLC and Mia Motors, Inc. He has conducted extensive research and has published more than 100 journal papers. He has taught tutorials and seminars on the subject of HEVs/PHEVs for the Society of Automotive Engineers (SAE), the IEEE, workshops sponsored by the National Science Foundation, and the National Society of Professional Engineers. He has delivered courses to major automotive OEMs and suppliers, including GM, Ford, Chrysler, Honda, Hyundai, Tyco Electronics, A&D Technology, Johnson Controls, Quantum Technology, Delphi, and the European Ph.D. School. He has offered tutorials in many countries, including the U.S., China, Korea, Singapore, Italy, France, and Mexico. He has published more than 100 articles and delivered 30 invited talks and keynote speeches. He has also served as a panelist in major IEEE and SAE conferences. His research interests include electric drives, power electronics, electric machines, renewable-energy systems, and electrical and hybrid vehicles.

Dr. Mi received the "Distinguished Teaching Award" and the "Distinguished Research Award" of University of Michigan, Dearborn. He also received the 2007 IEEE Region 4 "Outstanding Engineer Award," "IEEE Southeastern Michigan Section Outstanding Professional Award," and the "SAE Environmental Excellence in Transportation."